

Research report
Open

Corrosion modelling in new concrete types

Report number. KIMAB 2018-171

Title Corrosion modelling in new concrete types
Authors Tommy Zavalis, Andrew Gordon, Bror Sederholm, Jan Trägårdh, Luping Tang
Publication date October 2018
Report number KIMAB 2018-171
Status Open
Project number 15150
Department Corrosion
Research Area Bygg
Financing Vinnova / InfraSweden2018
Distribution Open
Approved by 2018-11-02

X 

Signerat av: Olivier Rod
Department manager

Corrosion modelling in new concrete types

Tommy Zavalis, Andrew Gordon, Bror Sederholm, Jan Trägårdh, Luping Tang

Report number KIMAB 2018-171

Abstract

In this report, an attempt to utilize mechanistic models to simulate corrosion on rebars in new concrete compositions in road environments was made. The model as a tool for improving the corrosion resistance of new types of concrete compositions was evaluated as well.

The mechanistic model was able to simulate variations of local pH, chloride concentration, wetting, oxygen dissolution and potential until initiation of corrosion occurred, when modelling parameters were available. For instance, inclusion of slag was shown to delay the initiation while increased porosity seemed to speed up the process. A very simplified 2D model setup also displayed the importance of accounting every boundary of concrete in contact with the atmosphere correctly in the simulations. The same model also showed that voids in the concrete influenced the initiation of corrosion.

The low availability of validation experiments and model parameters narrowed this work considerably. The mechanistic model as a tool for corrosion resistance testing of new types of concrete was therefore concluded to require further development.

Table of contents

| | | |
|-------|---------------------------------|----|
| 1 | Introduction..... | 1 |
| 2 | Theory..... | 2 |
| 2.1 | Equations | 2 |
| 2.1.1 | Governing Equations | 2 |
| 2.1.2 | Boundary Conditions | 3 |
| 2.1.3 | General Model Assumptions | 5 |
| 2.1.4 | Model Parameters | 5 |
| 2.1.5 | Model Geometry | 8 |
| 2.1.6 | Service-Life Exposure | 9 |
| 3 | Results and Discussion | 10 |
| 3.1 | 1D Model..... | 10 |
| 3.2 | 2D Model..... | 15 |
| 3.3 | Future work..... | 19 |
| 4 | Conclusions..... | 20 |
| 5 | List of symbols..... | 21 |
| 6 | Acknowledgments | 22 |
| 7 | References..... | 22 |

1 Introduction

The corrosion of reinforcement bars in concrete contributes considerably to limit the life time of concrete structures. Several factors affect the corrosion: surroundings, concrete properties and the design of the construction.

The binder mixture is of great importance for the reinforced concrete. It determines its strength, corrosion resistance, cost, and environmental impact. A quick and reliable method to evaluate different binders is therefore of utmost significance.

Modelling is a method that is used to evaluate concrete types in terms of their impact on rebar corrosion. Typical models used today are: ERFEC, Mejlbro-Poulsen's, DuraCrete, and ACI Life 365. All offer fast ways to calculate chloride concentration profiles mainly in 1D and use a diffusion coefficient that is corrected for one or more properties prone to change in exposed concrete in an empirical way [1]. For modelling of 1D+ systems and at the same time account for most species, reactions (chemical and electrochemical), transport mechanisms, and atmospheric conditions, mechanistic models have been used to some extent [2] [3] [4] [5]. These usually take longer to solve and require numerous parameters, but have the advantage of being able to show details in several dimensions over time.

This report uses a mechanistic model accounting for homogeneous reactions, mass transport, wetting and passive current to study three types of intact (uncracked) concretes. The simulations are limited both for simplicity and due to the lack of parameters available to the point when the initiation of corrosion takes place. The model incorporates also the dissolution of carbon dioxide into the pore liquid of the concrete, thereby accounting for both initiation of corrosion through chloride ingress and carbonation [6]. One year of exposure in a road environment is modelled. The cycle is based on one year of a published 10 year concrete exposure report [7] and accounts for variations in temperature, relative humidity, salt spraying, and rain. The comparisons of the concrete mixtures are mainly performed with a 1D model. Geometric effects are also studied for one of the mixtures with a simplified 2D model.

2 Theory

The mechanistic model in this report considers the electrochemical driving force imposed on species in the pores of a number of uncracked concrete types. All presented symbols are listed in chapter 5.

2.1 Equations

2.1.1 Governing Equations

The model solves mass balances for each species, i , in porous media, expressed as [8]:

$$\frac{\partial(\theta_w c_i)}{\partial t} = -\nabla \cdot (N_i) \quad (1)$$

The flux, N , of each species is derived from the electrochemical driving force, as described by the Nernst-Planck equation:

$$N_i = -\theta_w^\tau \cdot \frac{c_i D_i}{RT} \nabla \mu_i \approx -\theta_w^\tau \cdot D_i \nabla c_i - c_i \theta_w^\tau \cdot D_i \frac{z_i F}{RT} \nabla V \quad (2)$$

As the transport of species within the concrete is a convective diffusion problem, an additional flux term needs to be added to Eq. 2. This accounts for the convective flux within the water-filled pores [5], given by

$$N_{convection} = D_w(\theta_w) \nabla \theta_w \nabla c_i \quad (3)$$

The volume fraction of pore liquid, θ_w , is defined by Richard's equation and includes capillary water diffusivity in aged concrete:

$$\frac{\partial \theta_w}{\partial t} = \nabla \cdot (D_w(\theta_w) \nabla \theta_w) \quad (4)$$

$D_w(\theta_w)$ is the water-saturation dependent diffusion coefficient, given by:

$$D_w(\theta_w) = 2.2 \cdot 10^{-10} \cdot e^{6.4 \left(\frac{\theta_w - \theta_{wi}}{\theta_{wd} - \theta_{wi}} \right)} \quad (5)$$

The electric potential in the pore liquid is calculated from the conservation of charge, described by:

$$\nabla \cdot i = 0 \quad (6)$$

where the current density in the liquid is computed from the sum of fluxes of charged species, given by:

$$i = F \cdot \sum_i z_i \cdot N_i \quad (7)$$

To account for any non-ideality of the liquid, the concentration is multiplied with the activity coefficient to get the activity:

$$a_i = \gamma_i \cdot c_i \quad (8)$$

The activity coefficient is computed from by Davies' law, expressed as [9]:

$$\log(\gamma_i) = -0.51 \cdot z^2 \left(\frac{\sqrt{I}}{1+\sqrt{I}} - 0.2 \cdot I \right) \quad (9)$$

where the ionic strength of the pore liquid is calculated from:

$$i = 0.5 \cdot \sum_i z_i^2 \cdot c_i \quad (10)$$

Chloride is bound to different degrees on the pore walls of the concrete. The amount of bound chloride is proportional to the tricalcium-aluminate (C₃A) content of the cement. This content varies with the composition of the cement. A Langmuir type expression is used to describe the relation between bound, C_b, and free, C_f, chloride in the pores, described by:

$$C_b = \frac{\alpha C_f}{1 + \alpha C_f} \quad (11)$$

The constant α in eq. 11 changes with the content of Portland cement, blast furnace, and fly ash in the binder [4].

2.1.2 Boundary Conditions

At the rebar:

Oxygen reduction and iron dissolution take place on the rebar. A flux dependent on the passive current of the iron rebar is placed on the boundary for the liquid phase given by:

$$N_i = -\frac{i_p}{n_e F} \cdot \theta_w \quad (12)$$

The potential in the electrolyte is dictated by the passive current at the rebar ($i=i_p$).

At the outer boundaries of the concrete:

The pore water is assumed to be saturated with dissolved oxygen and carbon dioxide at the outer boundary (c.f. Table 2).

Evaporation of water takes place for the pore liquid at the boundary as well and depends on composition (water activity, a_w) and relative humidity of the surrounding atmosphere, as described by [10]:

$$N_{\theta} = -k_v \cdot (a_w - RH) \quad (13)$$

Eq. 13 assumes that while pore water exits by means of evaporation, the ions accompany the water to the surface and are removed from the concrete pores. The model also accounts for rainfall and salt spraying. For the former, the water flux is determined by the following simplification, which approaches zero as the pores are filled (i.e. volume fraction of pore liquid equals the concrete porosity, ε):

$$N_{\theta} = k_{rain} \cdot (\varepsilon - \theta_w) \quad (14)$$

For salt spraying no evaporation is assumed. Species containing iron and calcium are (when available) set to be washed out only during rain fall at the same rate as filling of the pores. The rain and spray are assumed to be saturated with carbon dioxide and oxygen.

The entry of chlorides to the concrete is modeled in a manner that accounts for the binder composition, given by [4]:

$$N_{Cl} = -1 \cdot 10^{-3} \cdot (c_{Cl} - c_s) + K_{Cl} \left(\frac{c_{Cl}}{-0.51} \right)^2 e^{-1.15c_{Cl}} \quad (15)$$

During rainfall, the second term in eq. 15 changes sign and the outside concentration is set to a low value. Eq. 15 sums diffusional and adsorption driving forces which determine the inflow of chlorides. K_{Cl} depends on binder composition.

The potential in the electrolyte is set as a reference (zero) at the outer boundary.

2.1.3 General Model Assumptions

In all calculations several assumptions are made.

- Only the point until initiation of rebar corrosion can be investigated. I.e. the pore liquid composition is studied without any influence of passivity changes and active corrosion of the rebar.
- Self-healing and buffering capacities of the binder (solid) is not studied either [11].
- The exposed reinforced concrete is completely hydrated at the start of the computations.
- Formation and reactions of solid species, e.g. Ca(OH)_2 and CaCO_3 [12], are for simplicity neglected.
- Any change in the volume fraction of the pore solution due to precipitation of salts and/or chloride binding is neglected [12] [2].
- Carbonization takes place due to dissolution of carbon dioxide into the pore solution at the surface of the concrete and is said to affect the carbonate concentration and pH of the liquid only.
- The pore walls do not affect the electroneutrality of the pore solution.
- Traces (or low concentrations) of cations, other than iron ions, are not included. Potassium ions [13] [14], typically not involved in any reactions [12], are for simplicity included in the sodium concentration.
- Despite the fact that sulphides are present in binders containing slag [14], these are for simplicity and due to the lack of modelling parameters not accounted for.
- No evaporation of water takes place within the pores of the concrete.
- The gas-liquid equilibriums for oxygen and carbon dioxide are only modelled at the surface of the concrete. To incorporate gaseous exchange within the pores, the diffusion coefficients are corrected as tabulated in Table 4.

2.1.4 Model Parameters

Species present in the pore liquid are tabulated in Table 1, the values are based mainly on reference [13] and coincide well with other observations [2]. Aside from these values, the pores are said to be completely filled with liquid initially. No cracks are at any time present in the concrete.

Table 1. Initial values in the pore liquid.

| Species | Value |
|-------------------|---------------------------------|
| Na^+ | 154 mol/m ³ |
| Ca^{2+} | 0.9 mol/m ³ |
| OH^- | 151 mol/m ³ (~pH 13) |
| Cl^- | 2 mg/l |
| Fe^{2+} | 0.02 mol/m ³ |
| O_2 (aq) | 0.01 mol/m ³ |

The species are involved in numerous reactions, as shown in Table 2.

Table 2. Reaction system [15] [16].

| <i>Reaction</i> | <i>Equilibrium constant (K) / Solubility constant (K_s) / Henry constant (H)</i> |
|--|--|
| $\text{H}^+ + \text{OH}^- \leftrightarrow \text{H}_2\text{O}$ | $\log K = -14$ |
| $\text{CO}_2(\text{g}) \leftrightarrow \text{CO}_2(\text{aq})$ | $H = 3.39 \cdot 10^{-2} \text{ M/atm}$ |
| $\text{CO}_2(\text{aq}) + \text{H}_2\text{O} \leftrightarrow \text{H}_2\text{CO}_3$ | $\log K = -2.55$ |
| $\text{H}_2\text{CO}_3 \leftrightarrow \text{HCO}_3^- + \text{H}^+$ | $\log K = -6.34$ |
| $\text{HCO}_3^- \leftrightarrow \text{CO}_3^{2-} + \text{H}^+$ | $\log K = -10.33$ |
| $\text{Ca}^{2+} + \text{H}_2\text{O} \leftrightarrow \text{CaOH}^+ + \text{H}^+$ | $\log K = -12.697$ |
| $\text{Ca}^{2+} + \text{H}^+ + \text{CO}_3^{2-} \leftrightarrow \text{CaHCO}_3^+$ | $\log K = 11.599$ |
| $\text{Ca}^{2+} + \text{CO}_3^{2-} \leftrightarrow \text{CaCO}_3$ | $\log K = 3.20$ |
| $\text{Fe}^{2+} + \text{H}_2\text{O} \leftrightarrow \text{FeOH}^+ + \text{H}^+$ | $\log K = -9.5$ |
| $\text{Fe}^{2+} + 2\text{H}_2\text{O} \leftrightarrow \text{Fe}(\text{OH})_2 + 2\text{H}^+$ | $\log K = -20.6$ |
| $\text{Fe}^{2+} + 3\text{H}_2\text{O} \leftrightarrow \text{Fe}(\text{OH})_3^- + 3\text{H}^+$ | $\log K = -31$ |
| $\text{Fe}^{2+} + 4\text{H}_2\text{O} \leftrightarrow \text{Fe}(\text{OH})_4^{2-} + 4\text{H}^+$ | $\log K = -46$ |
| $\text{Fe}^{2+} + \text{Cl}^- \leftrightarrow \text{FeCl}^+$ | $\log K = -0.20$ |
| $\text{Fe}^{2+} + 2\text{Cl}^- \leftrightarrow \text{FeCl}_2$ | $\log K = -2.45$ |
| $\text{Fe}^{2+} + 4\text{Cl}^- \leftrightarrow \text{FeCl}_4^{2-}$ | $\log K = -1.91$ |
| $\text{Fe}^{2+} + \text{CO}_3^{2-} \leftrightarrow \text{FeCO}_3$ | $\log K = 3.20$ |
| $\text{Na}^+ + \text{H}^+ + \text{CO}_3^{2-} \leftrightarrow \text{NaHCO}_3$ | $\log K = 10.079$ |
| $\text{Na}^+ + \text{CO}_3^{2-} \leftrightarrow \text{NaCO}_3^-$ | $\log K = 1.270$ |

Physical parameters and diffusion coefficients are tabulated in Table 3 and Table 4, respectively. Detailed assumptions and descriptions of parameter usage are found in the “Comment” columns.

Table 3. Physical parameters.

| Parameter | Value | Comment |
|---------------|-----------------------|--|
| i_p | 0.01 A/m ² | [2] |
| k_{rain} | 1 | Assumed value. |
| k_v | 1.5e-8 m/s | Fitted to reference [17]. |
| m_{binder} | 380 kg/m ³ | Value taken from [7]. |
| w/c | 0.5 | Value taken from [7]. |
| ε | 0.1 | Normally between 0.1 and 0.15 [18] [19]. |
| θ_{wi} | 1.5 | Based on the water-cement ratio [5]. |
| θ_d | 0.15 | Saturated water content is approximated to be the same as the fully filled pore volume, $\theta_d = \varepsilon$. |
| τ | 2.5 | [20] |

Table 4. Diffusion coefficients. All iron compounds not listed are set to have the same value as free iron ions.

| Property | Value / m ² s ⁻¹ | Comment |
|--------------|--|---|
| DNa^+ | $1.33 \cdot 10^{-9}$ | From mobility at 298 K [21]. Temperature dependence included in model. |
| DCl^- | $2.03 \cdot 10^{-9}$ | .. |
| $DFeCl^+$ | $8.00 \cdot 10^{-10}$ | .. |
| $DFeCl_2$ | $1.00 \cdot 10^{-9}$ | .. |
| $DFeCl_4$ | $1.10 \cdot 10^{-9}$ | .. |
| $DFeOH^+$ | $7.50 \cdot 10^{-10}$ | .. |
| $DFe(OH)_2$ | $7.80 \cdot 10^{-10}$ | .. |
| DH^+ | $9.30 \cdot 10^{-9}$ | .. |
| DOH | $5.30 \cdot 10^{-9}$ | .. |
| DCO_3^{2-} | $9.22 \cdot 10^{-10}$ | .. |
| $DHCO_3^-$ | $1.18 \cdot 10^{-9}$ | .. |
| D_w | $2.2 \cdot 10^{-10} e^{6.4 \left(\frac{\theta_w - \theta_{w0}}{\theta_{wd} - \theta_{w0}} \right)}$ | [5] |
| DO_2 | Function of θ_w/ε | Value increases with less liquid in pores [22]. |
| DH_2CO_3 | $1.92 \cdot 10^{-9} \cdot DO_2(\theta_w = \varepsilon) / DO_2(\theta_w/\varepsilon)$ | Value from reference [21] corrected as for DO_2 to roughly approximate for better transport of carbon dioxide in liquid-free part of the pores. |

2.1.5 Model Geometry

The model dimensions are set to approximately the same dimensions as the slabs in the report by Tang et al. [7]. Figure 1 shows a schematic image of the modelled concrete with its pores partially filled with liquid and some species in the aqueous and gaseous phases.

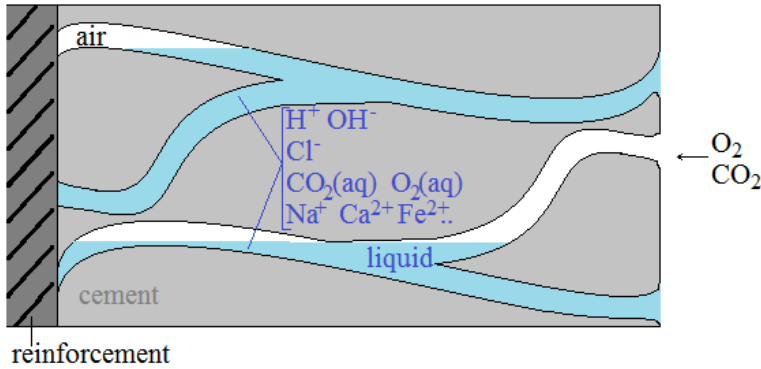


Figure 1. Schematic illustration of a fraction of a reinforced concrete slab with some crucial species.

The system above is modelled first in a detailed 1D model from the reinforcement surface to the concrete-atmosphere boundary. The distance, equal to the concrete cover thickness, is set to 0.05 m in the model.

A simplified 2D model is also used. The geometric dimensions are in the same order as the 1D model and it simulates a rebar situated in an asymmetric way in relation to possible concrete-atmosphere (outer) boundaries. The 2D model is both solved with the geometry in Figure 2a for study of species entry/exit boundaries and with the one in Figure 2b to investigate how voids beneath the rebar, as discussed by Zhang et al. [19], may influence the initiation of corrosion.

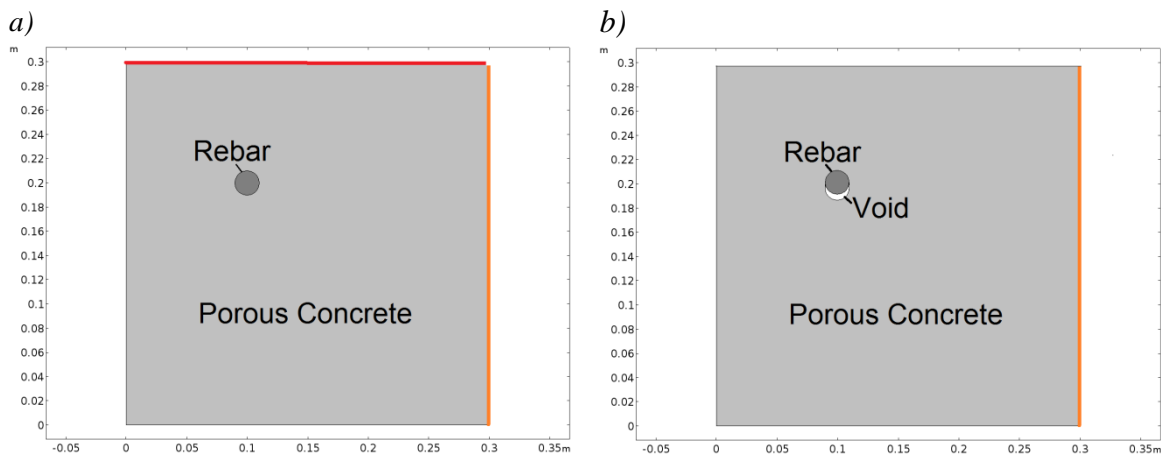


Figure 2. 2D model geometry a) without and b) with void beneath rebar. Coloured boundaries indicate concrete-atmosphere boundaries.

2.1.6 Service-Life Exposure

The model uses information from reference [7] for Highway 40 in Sweden together with data from the Swedish Meteorological and Hydrological Institute (SMHI) [23] to simulate the service life behaviour of concrete in a road environment during one year. The service life conditions accounted for in the model are displayed in Figure 3. The data applies for the city of Borås, which is situated on Highway 40, during one year (Aug. 2001 - July 2002). The temperature and relative humidity (RH) are one day averages. The salt spraying is assumed to take place continuously from November up until February and the spray that reaches the concrete is said to contain 1 wt% of NaCl salt solution. A concentration of 1 wt% is selected since it fits what is typically used in accelerated corrosion tests (ACTs). Borås has approximately 15 days with rain each month. As a simplification, the model sets rain conditions during the latter half of each month.

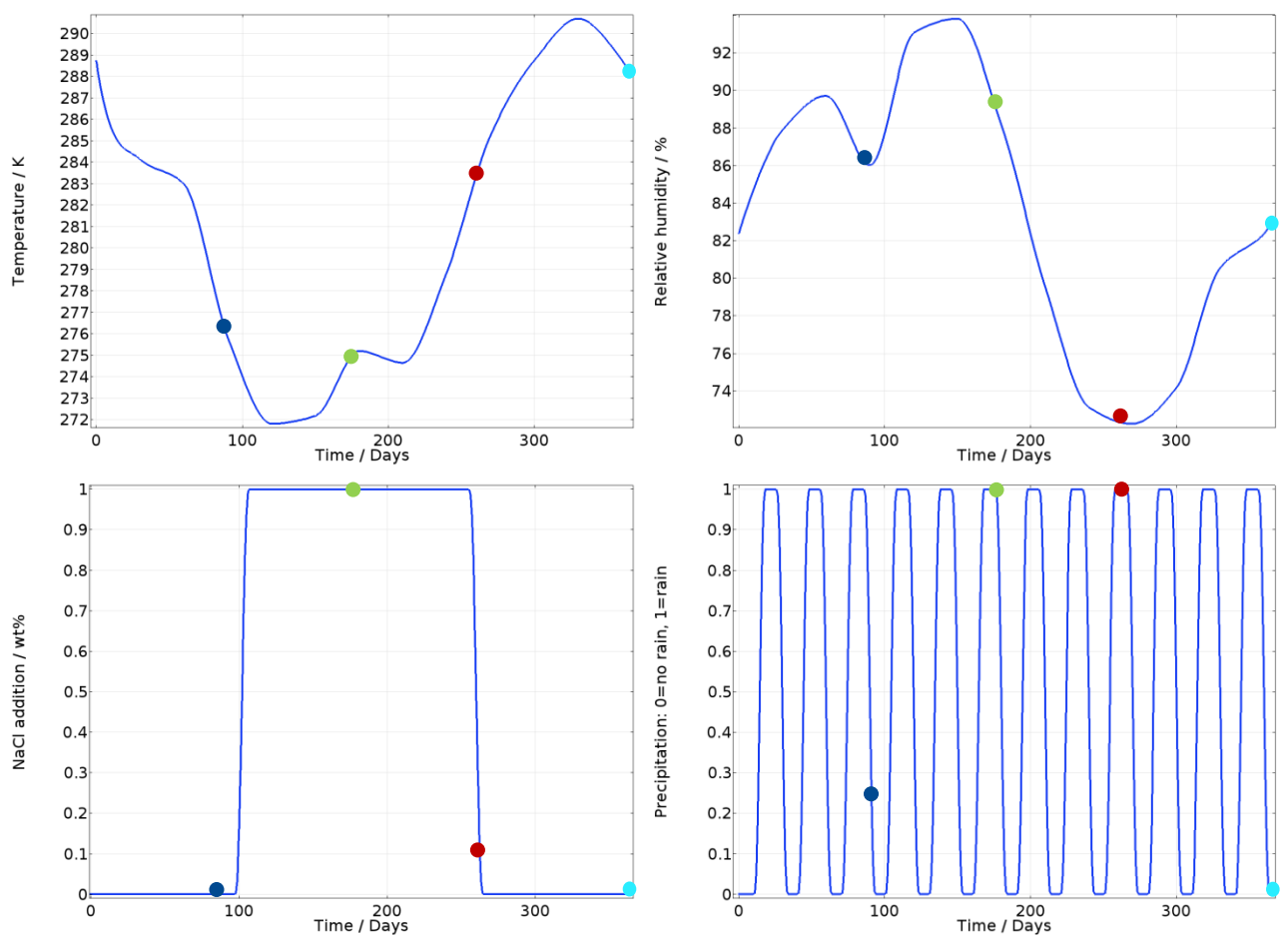


Figure 3. Temperature, relative humidity, salt spraying, and precipitation from August 2001 up until July 2002. Coloured dots indicates times, 3 months, 6 months, 9 months and one year, at which the results are plotted.

3 Results and Discussion

The results presented are for three types of binder mixtures:

- 1) 100% Portland cement (or 100% “anläggningscement” [7])
- 2) Portland cement with 12.5% blast furnace slag (similar to Finnish standard Portland cement with 10-15% blast-furnace slag [7])
- 3) Portland cement with 12.5% blast furnace slag with higher porosity than cement “2”.

Initial conditions, water-cement ratios and binder masses are the same in all three mixtures. The second mixture is included to investigate the impact of new binders and the third to investigate a supposed change in concrete porosity with the introduction of slag into the binder. Since the dependence of porosity and slag content is unclear [24], a higher porosity is selected arbitrarily (from 0.1 to 0.15).

3.1 1D Model

Figure 4 shows the variation of chloride concentration, pH, dissolved oxygen, and wetting of pores for concrete according to mixture 1. The colours of the curves plotted against distance from the reinforcement (or rebar) correspond to the point in time indicated in Figure 3.

Reported chloride concentration thresholds for corrosion initiation (0.2-0.4 % weight of binder [25] [11]) are not surpassed during this year of exposure. The pH decreases to some extent near the rebar, but should not be a source for corrosion initiation as it does not fall below 11.75, which is the value mentioned by Scott et al. [14] as the lowest pH at which rebars are fully passivated in aqueous solution and thus are unlikely to corrode. The oxygen concentration at the rebar, critical for the oxygen reduction reaction involved in corrosion, is near zero even for the passive current and indicates that the transport of oxygen will limit corrosion. The wetting of the pores is shown to be even within the slab and changes considerably with time. However, the exposure simulated in this report does not seem to completely dry out the slab which limits the transport of gases to the rebar.

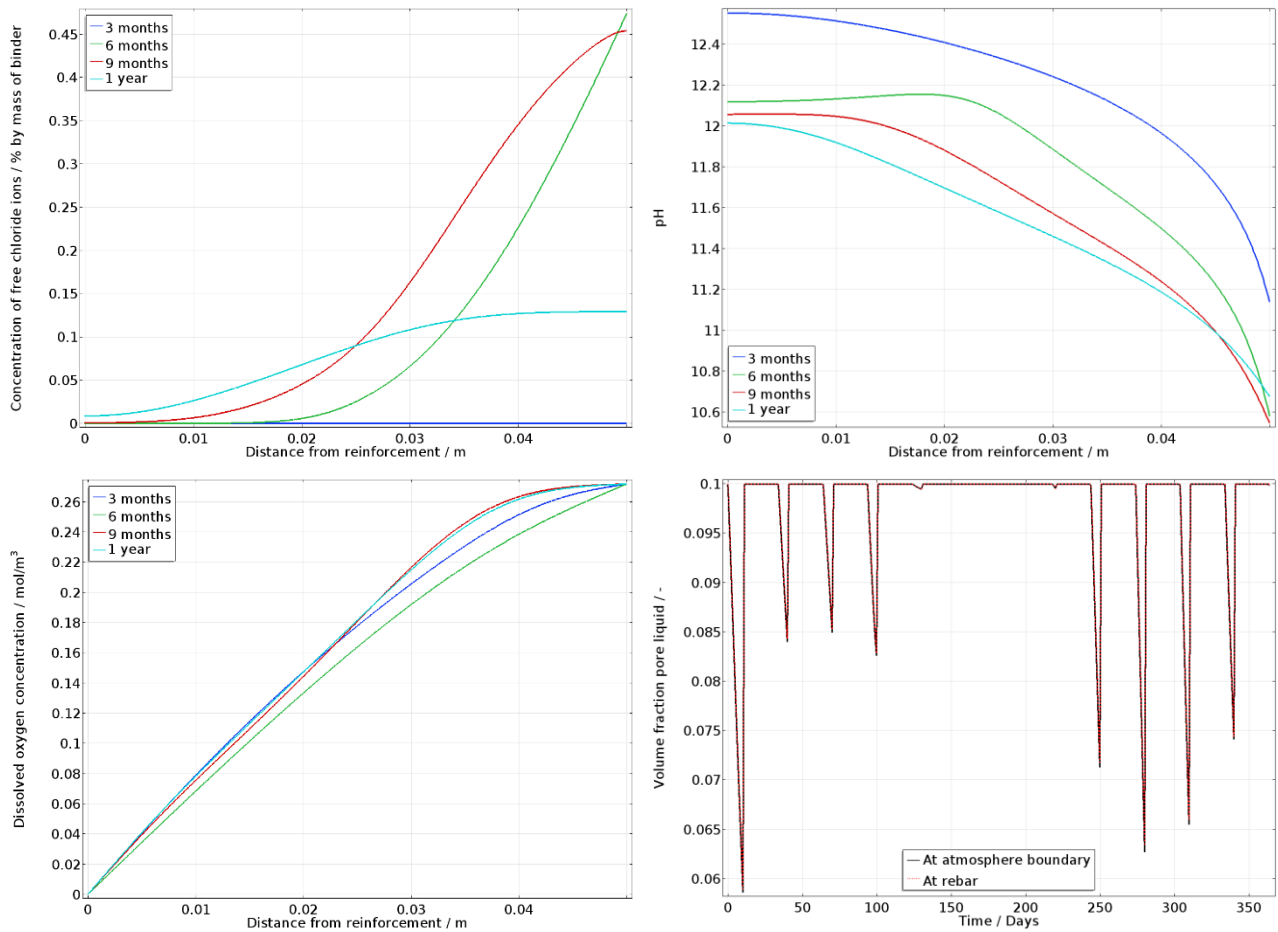


Figure 4. Chloride concentration, pH, dissolved oxygen concentration, and volume fraction of pore liquid for mixture 1.

In Figure 5 simulation results are shown for mixture 2. The differences with mixture 1 are very small, especially in regards to oxygen concentration and wetting. However, after 1 year the variations in chloride concentration near the rebar are slightly lower and the pH slightly higher. This shows that the small slag-content in the concrete in mixture 2 possibly delays or even prevents the initiation of corrosion. The explanation is mainly the chloride binding isotherm used in the model that increases the chloride binding to the pore walls with the addition of slag to the binder mixture. These results are in line with the results presented in reference [7] that show small differences between the two slabs after 10 years (slab 202 compared to 212 in Table 3.2). However, the wetting behavior deviates; the measurements show clear discrepancies between the mixtures which may be a consequence of the model setup, the simulated exposure cycle, or the fact that only one year is simulated. Decrease in free chloride-ion concentration near the rebar with slag content has been reported previously [26] [4] [24]. The free chloride concentration values along the depth of the slabs are in the same magnitude as what has been seen for cement slabs exposed in road environment for one year [27].

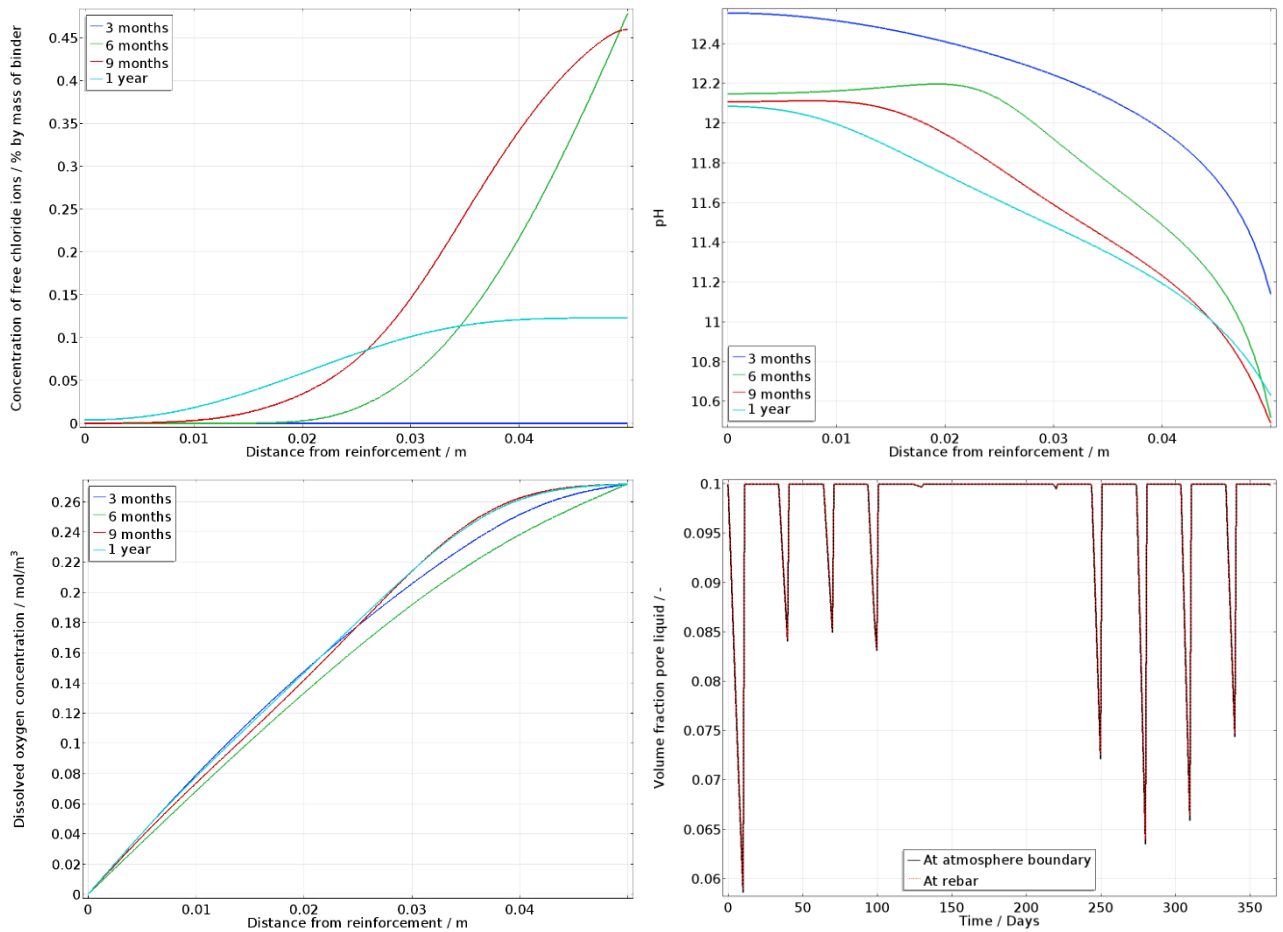


Figure 5. Chloride concentration, pH, dissolved oxygen concentration, and volume fraction of pore liquid for mixture 2.

Mixture 3 varies from the two previous mixtures as is displayed in Figure 6. The chloride ingress in particular is greater; around the threshold for corrosion initiation. This is a result of the increased effective diffusion provided by the higher porosity and wetting ($DCl_{eff} = \theta_w^\tau \cdot DCl$). The oxygen concentration profile is similar to mixtures 1 and 2, and shows that the corrosion is limited for mixture 3 as well. However, the total amount of oxygen reaching the rebar over time is higher causing more oxygen reduction and thus iron dissolution at the rebar (increased passive current corrosion). This is clearly indicated by the lowered pH at the rebar resulting from the iron hydrolysis. The overall drop in pH in the concrete cover is also a result of more carbonation due to faster ingress of carbon dioxide. Thus, all species move more efficiently in the larger pores presenting the concrete porosity to be a very important property in regards to rebar corrosion. It should be noted, that since the passive layer breakdown is not included in the model, the high chloride concentration probably affects the concrete more than observed in Figure 6 after some time. However, the results still indicate that the time for corrosion initiation is the shortest for mixture 3.

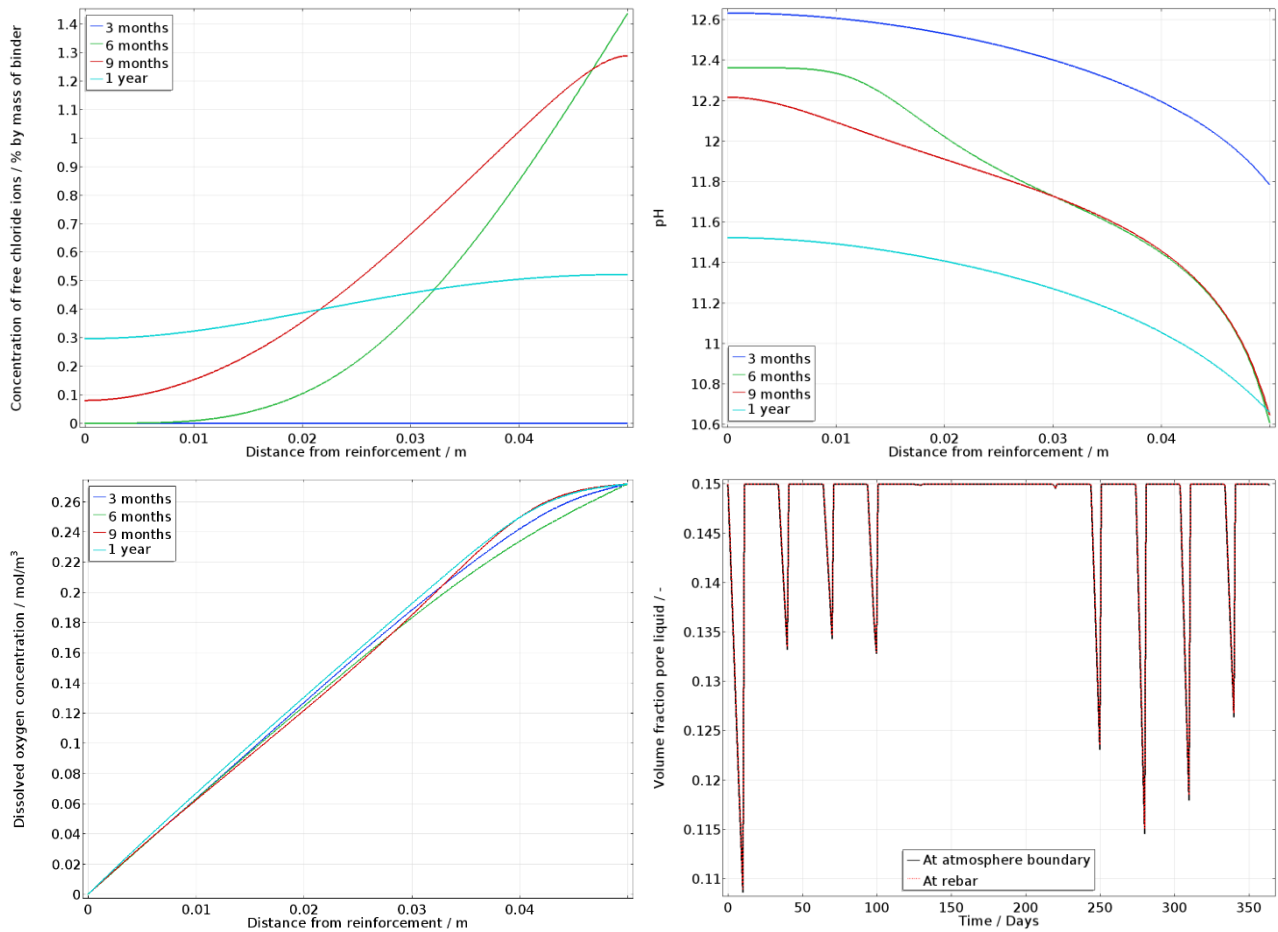
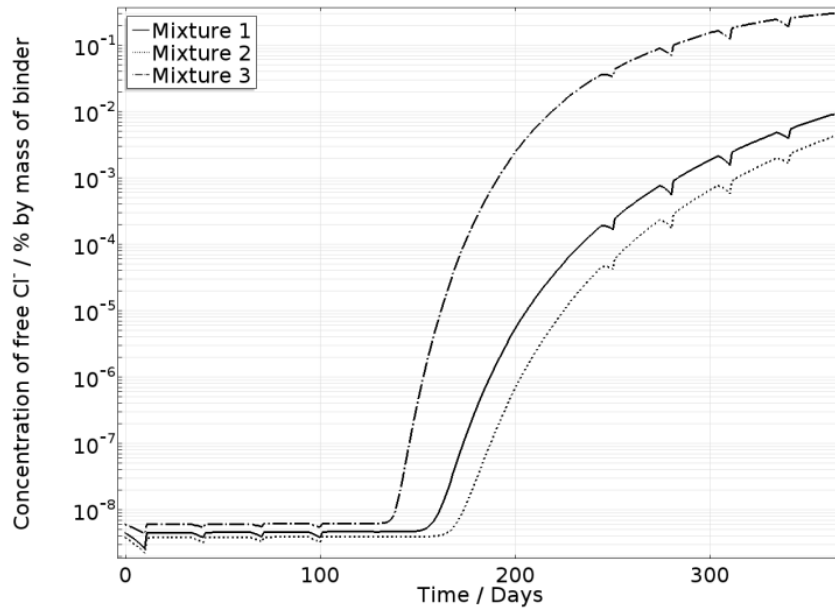


Figure 6. Chloride concentration, pH, dissolved oxygen concentration, and volume fraction of pore liquid for mixture 3.

The free chloride-ion concentrations near the rebar are shown in Figure 7a. As mentioned before, most chlorides have reached the rebar in mixture 3 and least in mixture 2. Another relevant measurement of corrosion initiation is found in Figure 7b; the molar ratio between free chloride-ion concentration and hydroxide concentration. The differences between the three mixtures are more clearly shown here. Scott et al. [14] mention ratios between 0.25 to 1.08 to induce corrosion in aqueous solution. In regards to this, all the mixtures studied here could suffer from rebar corrosion. This may also explain why indications of corrosion have been seen for mixture 1 (slab 202, Table 3.2 in reference [7]).

a)



b)

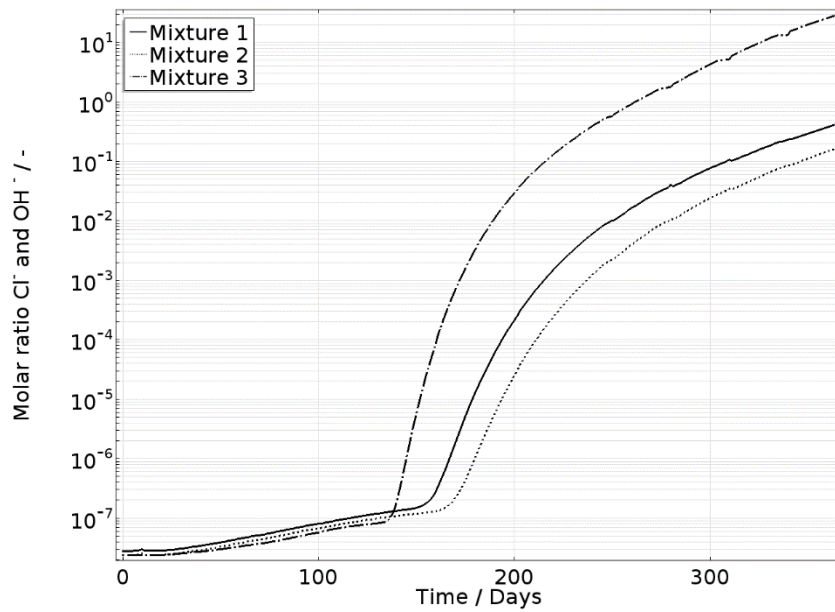


Figure 7. Concentration of free chloride ions. b) Molar ratio free chloride ions and hydroxide concentrations at the rebar.

3.2 2D Model

The 2D model is considerably simplified compared to the 1D model. This was a necessary measure to reduce computation time and computer memory usage. The simplifications were made in accordance with the results so far. Since little variation between mixtures 1 and 2 was shown in regards to pH and oxygen transport, the 2D model is only solved for bound and free chloride-ion concentrations and the volume fraction of the pore liquid. The model investigates how the most corrosion resistant mixture (mixture 2) behaves when some geometrical features are accounted for. The tortuosity (τ) and evaporation/condensation rate constant (k_{vap}) are set to 1.5 and $5 \cdot 10^{-8}$ m/s, respectively, in the model. The work presented here is a first step towards creating a reliable 2D model.

The effect of atmosphere-concrete boundaries on corrosion initiation is studied by simulating the cases with either one (boundary B, Figure 8) or two boundaries (boundaries A and B, Figure 8) in contact with atmosphere.

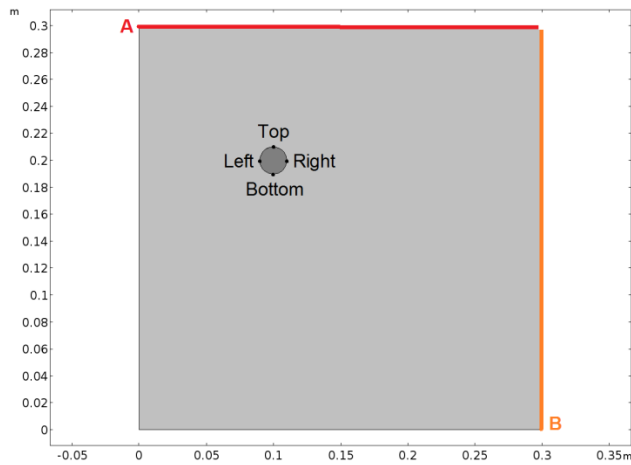


Figure 8. 2D model geometry used for investigation of different atmosphere-concrete boundaries.

Figure 9 shows that considerably more chlorides reach the rebar when both boundaries are in contact with the atmosphere.

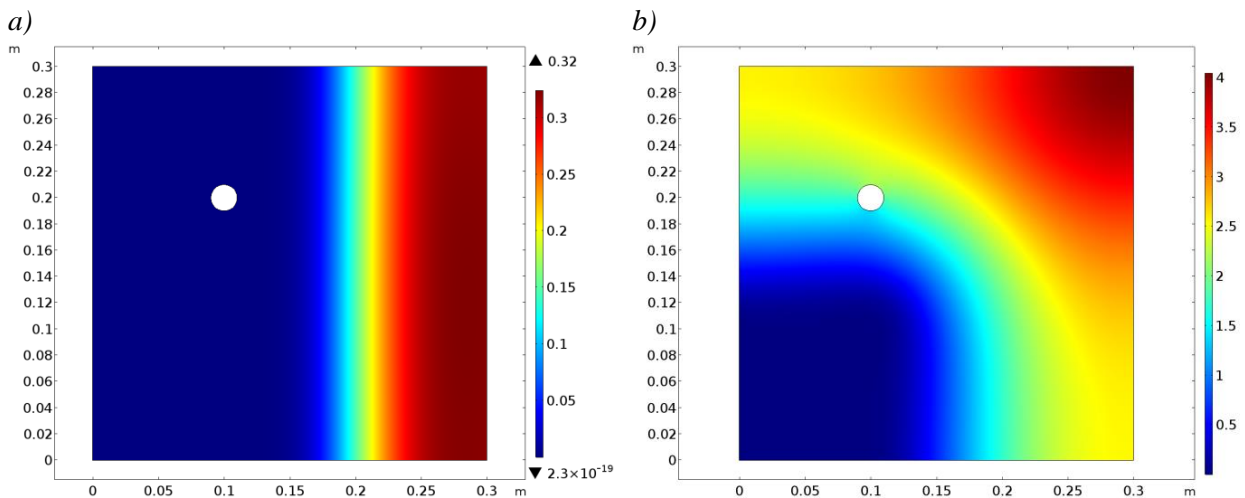


Figure 9. Concentration of free chloride ions after 1 year when a) boundary B and b) boundaries A and B are in contact with the atmosphere .

In Figure 10a, the concentration of free chloride ions at four locations around the rebar are shown for the case of two boundaries in contact with the surroundings. The values are considerably higher than for the case of one boundary, which do not surpass 0.001 wt%. Additionally, the distribution of chloride ions is very uneven with at least 1 wt% difference between the top and bottom of the rebar. As shown in Figure 10b, the drying of the concrete is doubled near the rebar. The variation in values around the rebar is very even in both cases, reaching a maximum difference of ~0.001 during the exposure.

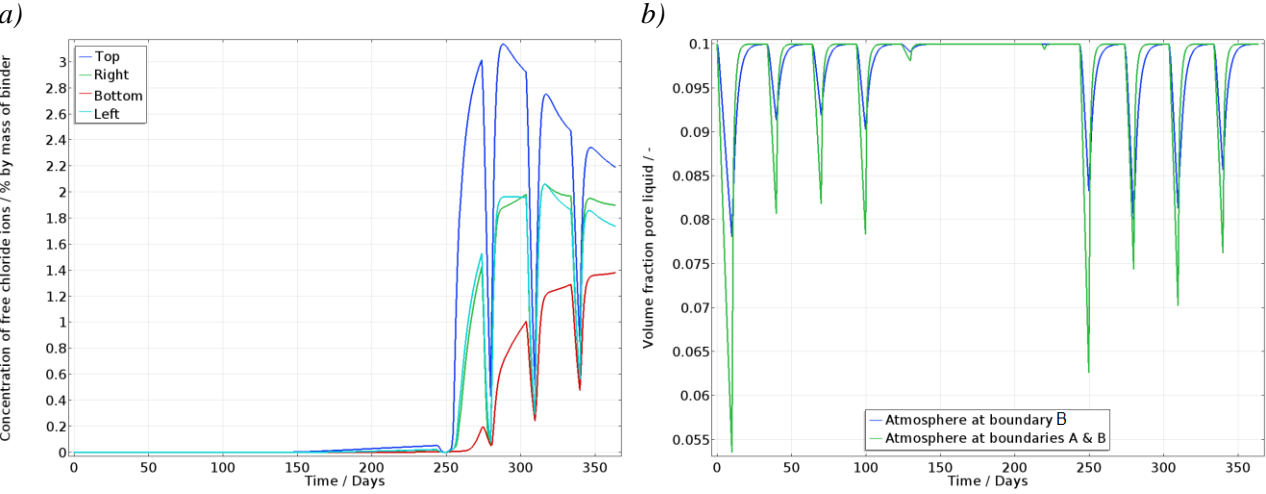


Figure 10. a) Free chloride-ion concentrations at the rebar when boundaries A and B are in contact with the atmosphere. b) Average of the volume fraction of pore liquid at the rebar for the two different atmosphere boundary cases.

The difference in wetting within the entire slab peaks at the end of drying periods without salt spraying (e.g. after 12 days in Figure 11), but is for the rest of the exposure quite evenly distributed. This shows a very efficient capillary flow of liquid in contrast to chloride transport. The low wetting intensifies the capillary flow from the surface when it rains or when salt spraying takes place; capillary flow being driven by the local gradients in the volume fraction of pore liquid [6]. Increased capillary flow from the surface during salt spraying increases the ingress of chlorides.

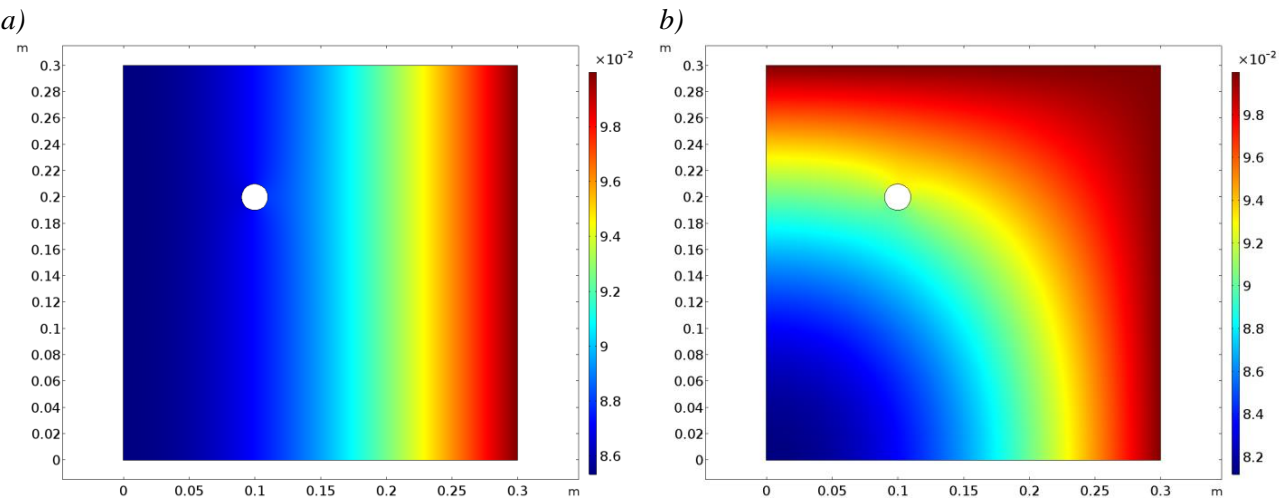


Figure 11. Volume fraction of pore liquid after 12 days when a) boundary B and b) boundaries A and B are in contact with atmosphere.

The presence of a void below the rebar, formed during the hardening of the concrete [19], is simulated for mixture 2 with the simplified 2D model as well. However, the present model setup only enables study of a void filled with liquid initially which may deviate from real conditions. An additional assumption is also required: The void is said to contain enough liquid to cover the boundary between the void and concrete with water for the whole exposure cycle, i.e. the volume fraction of pore liquid (θ_w) at that boundary is 0.1. Simulations are only performed for the case of one boundary in contact with atmosphere to ensure that the void is sufficiently wet. Figure 12 displays the model geometry with the additional assumption.

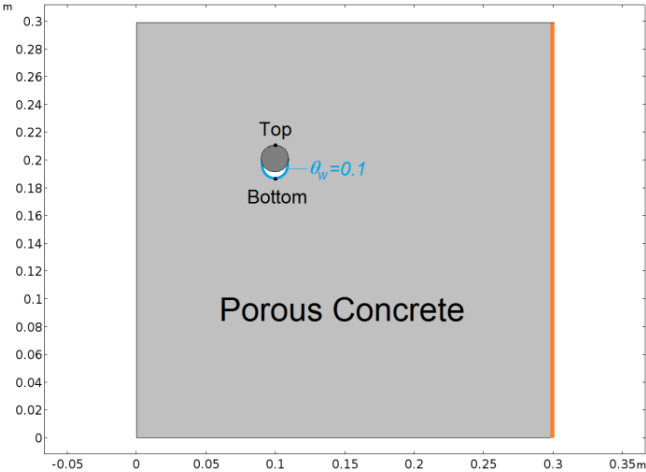


Figure 12. 2D model geometry with void and additional assumption of liquid in void marked.

The wetting of the concrete slab changes considerably with the presence of the void. As displayed in Figure 13 after 3 months of exposure, the wetting becomes more uneven compared to when no void is present. Also, the vicinity of the rebar tends to contain more liquid compared to the rest of the slab.

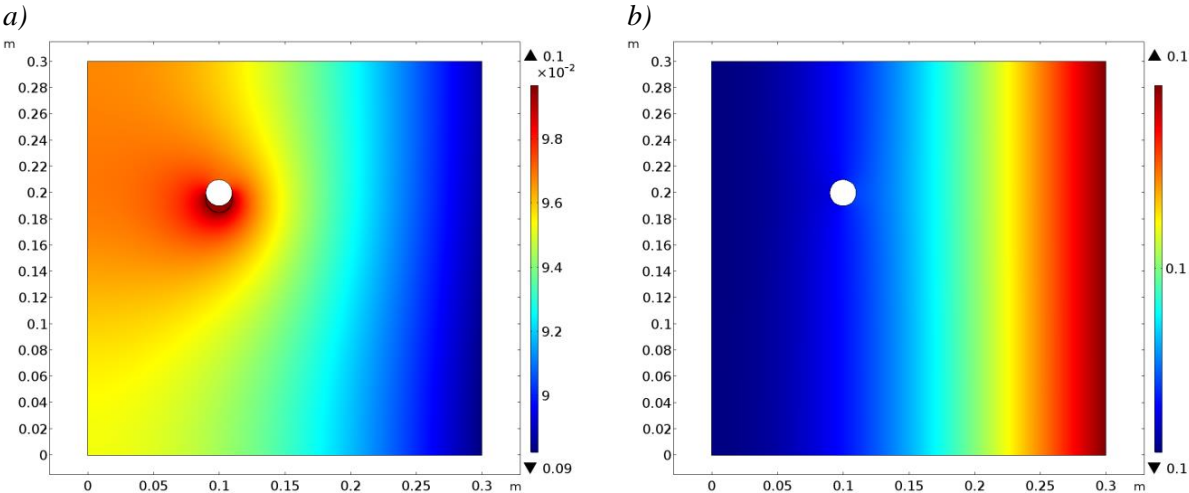


Figure 13. Volume fraction of pore liquid after 3 months a) with and b) without void beneath the rebar.

Figure 14 displays the volume fraction of pore liquid averaged along the atmosphere-concrete boundary. This shows the concrete to be more wetted with a liquid filled void.

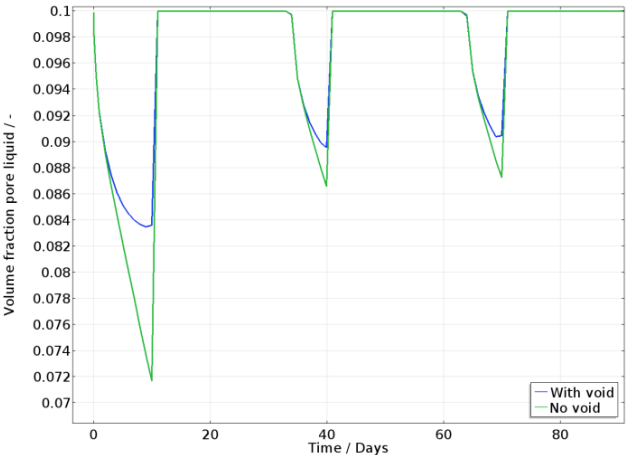


Figure 14. Average of the volume fraction of pore liquid at the atmosphere-concrete boundary (boundary B) during the three first months of exposure. Behaviour shown both with and without void.

As explained earlier, both capillary flow and consequently chloride-ion ingress increase when the concrete dries out before salt spraying. Figure 15 demonstrates this; the chloride concentration is much lower in the concrete with the void present (cf. Figure 9a).

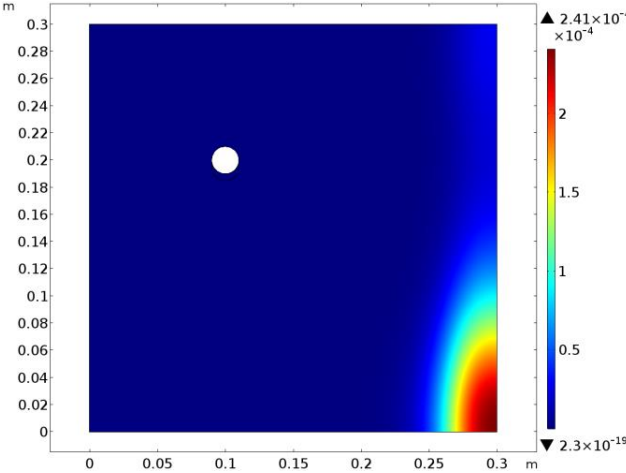


Figure 15. Concentration of free chloride ions after 1 year a) with void and b) without void beneath the rebar.

Since a liquid-filled void initially gives more liquid within the pores during the exposure, it is likely that a dry void initially dries up the concrete to some extent. This should be a source of higher chloride concentrations within and could explain why studies have shown voids to increase rebar corrosion in concrete [19].

3.3 Future work

The following has been identified within this report as a requirement for the development of reliable mechanistic models aimed as tools for investigation and improving the corrosion resistance of new types of concrete compositions:

- Experimental data for model validation purposes: The collection of relevant data often takes place in intervals of 6 months or more. This is not often enough for validation, especially if the data comes from concrete slabs in road environment where the variations in properties are much more frequent. Additionally, for new binder mixture compositions, 1D profiles (of at least two measuring points) within the concrete are critical for validation and scarcely exist for wetting and pH in any type of exposure environment.
- Salt spraying characteristics on concrete slab: The concentration and state of the chlorides reaching the concrete during salt spraying in e.g. road environment are not fully known, making it difficult to model.
- Modelling parameters: Mainly mass transport parameters such as diffusion parameters are vastly available as effective values including both porous and wetting effects. In order to use these, the porosity and/or wetting need to be known as well and this is seldom the case particularly for new binder compositions.
- Modelling features: The procedure of modelling voids is difficult to describe mathematically and validation experiments are lacking. The change of rebar passivity can be interesting when studying the initiation of corrosion, however, full explanations of this process is not available and hard to simulate.

The future work that needs to be done includes the production of adequate experimental data for validation purposes of new binder compositions. Ideally, such data should be from at least two measuring points within a reinforced concrete slab of known dimensions, composition, and porosity in salt solution of controlled concentration and temperature. If the concentration and temperature is possible to hold constant in such an experiment, collection of validation data at the beginning and end of exposure is sufficient. Most necessary data and modelling parameters can be retrieved from this type of experiment, but data on wetting needs to be collected in additional experiments as well.

For modelling and investigation of concrete under realistic conditions, measures need to be taken to fully understand how the salt spraying affects the surface and wetting of the concrete slab. Sensors placed on slabs in the field might be a solution.

If large voids in the concrete are to be accounted for in simulations, the model setup requires some tuning and, possibly, validation experiments. At the time being, the setup cannot simulate filling of voids. It might also be of relevance to try to solve the 2D model with full sets of properties (as the 1D model) to fully verify that the assumptions/simplification are valid. Other geometrical shapes and sizes together with more rebars per slab might also be of interest to examine. The long term aim is also to include the passive layer breakdown and corrosion propagation into the model and the interaction of solid species and liquid.

4 Conclusions

The conclusions from the attempt to utilize mechanistic models to simulate the initiation of corrosion in new concrete compositions in road environment are the following:

- The models are able to simulate details, such as local homogeneous reactions, pH, chloride concentration and transport of gases, relevant to the initiation of corrosion for three types of binder mixes in road environment.
- Geometric effects prove possible to study with 2D mechanistic models to some extent as well, but the model setup requires some simplifications.
- Slag in the binder mixture inhibits the initiation of corrosion. However, porosity has a larger impact on the initiation. If the porosity increases, the path for species transport in liquid opens up more allowing faster ingress of chlorides.
- The atmosphere-concrete boundaries of a concrete slab in road environment need to be accounted for in a correct manner in the model, since these dictate the wetting and chloride ingress.
- Voids that may have formed beneath the rebar affect the wetting of the concrete, possibly also affecting the corrosion initiation.
- At present, new types of concretes are only possible to simulate in a reliable way to a very small extent. This is due to the lack of model parameters and relevant experiments for model validation purposes, especially from other binder mixtures than Portland Cement.

5 List of symbols

| | | |
|---------------|---|---|
| a | activity | [mol m ⁻³] |
| a_w | activity of water | [mol m ⁻³] |
| c | concentration | [mol m ⁻³] |
| C_b | chloride concentration bound to the solid concrete matrix | [kg Cl/kg binder] |
| C_f | chloride concentration in pore liquid | [kg Cl/kg binder] |
| D | diffusion coefficient | [m ² s ⁻¹] |
| D_w | diffusion coefficient of capillary water | [m ² s ⁻¹] |
| F | Faraday's constant, 96487 | [As mol ⁻¹] |
| I | Ionic strength | [mol dm ⁻³] |
| i | current density | [A m ⁻²] |
| i_p | passive current density | [A m ⁻²] |
| K_{Cl} | adsorption flux constant dependent on binder type | [mol m ⁻² ·s ⁻¹] |
| k_v | rate of evaporation/condensation | [m/s] |
| k_{rain} | wash out rate at rain | [m/s] |
| m_{binder} | binder mass | [kg/m ³] |
| N | flux in pore liquid | [mol m ⁻² ·s ⁻¹] |
| N_θ | flux of water in pore liquid | [mol m ⁻² ·s ⁻¹] |
| N_{Cl} | flux of chlorides in pore liquid | [mol m ⁻² ·s ⁻¹] |
| n_e | number of electrons exchanged in reaction | [-] |
| R | universal gas constant, 8.3143 | [J mol ⁻¹ K ⁻¹] |
| RH | relative humidity | [-] |
| T | temperature | [K] |
| t | time | [s] |
| z | ion charge number | [-] |
| V | potential in pore liquid | [V] |
| γ | activity coefficient | [-] |
| ε | concrete porosity | [-] |
| θ_w | volume fraction of pore liquid (of whole concrete volume) | [-] |
| θ_i | initial water content (based on water-cement ratio) | [-] |
| θ_d | saturated water content | [-] |
| μ | electrochemical potential | [J mol ⁻¹] |
| τ | tortuosity | [-] |

6 Acknowledgments

Thanks to InfraSweden2030 and Vinnova for financing this prestudy.

7 References

- [1] L. Tang, "Validation of models for prediction of chloride ingrees in concrete exposed to a de-icing salt road environment," Chapter 7 of Book in Preparation
- [2] P. Ghods, "Multi-Scale Investigation of the Formation and Breakdown of Passive Films on Carbon Steel Rebar in Concrete," PhD Thesis, Department of Civil and Environmental Engineering, Carleton University, Ottawa, Canada, 2010.
- [3] C. Cao, "3D simulation of localized steel corrosion in chloride contaminated reinforced concrete," *Construction and Building Materials*, vol. 72, pp. 434-443, 2014.
- [4] Tetsuya Ishida, Prince O'Neill Iqbal, and Ho Thi Lan Ahn, "Modeling of chloride diffusivity coupled with non-linear binding capacity in sound and cracked concrete," *Cement and Concrete Research*, vol. 39, pp. 913-923, 2009.
- [5] J. Ozbolt, G. Balabanic, G. Periskic, and M. Kuster, "Modelling the effect of damage on transport processes in concrete," *Corrosion Science*, vol. 24, pp. 1638-1648, 2010.
- [6] C. Ljungkrantz, G. Möller, and N. Petersons, "Betonghandbok," 2nd Ed., Chapter 22 (K. Byfors and K. Tuutti), Svensk byggtjänst, Stockholm, 1994.
- [7] L. L. Tang. and P. Utgenannt, "Chloride Ingress and Reinforcement Corrosion in Concrete under De-icing Highway Environment – A study after 10 years' field exposure," SP Technical Research Institute of Sweden, Building Technology and Mechanics, SP Report 2007:76, Borås 2007.
- [8] J. S. Newman, "Electrochemical Systems," 2nd Ed., Prentice-Hall, U.S.A., 1991.
- [9] R. A. Robinson and R. H. Stokes, "Electrolyte Solutions," 2nd Ed., Dover publications, U.S.A., 2002.
- [10] C. Taxén, "KIMAB confidential report".
- [11] C. Sosdean, "Experimental and numerical investigations of the influence of cracks on mass diffusion in mortar and concrete," PhD Thesis, Polytechnic University of Timisoara, Romania, 2015.
- [12] B. Johannesson, "Transport and sorption phenomena in concrete and other porous media," PhD Thesis, Division of Building Materials, LTH, Lund University, 2000.
- [13] B. Lagerblad and J. Trägårdh, "Conceptual model for concrete long time degradation in a deep nuclear wate repository," 2:96, CBI Swedish Cement and Concrete Research Institute, Stockholm, Sweden, 1996.
- [14] A. Scott and M. G. Alexander, "Effect of supplementary cementitious materials (binder type) on the pore solution chemistry and the corrosion of steel in alkaline environments," *Cement and Concrete Research*, vol. 89, pp. 45-55, 2016.
- [15] MINEQL+ 4.6, Software program

- [16] C. F. Baes and R. S. Mesmer, "The Hydrolysis of Cations," Reprint Ed., Wiley, U.S.A., 1986.
- [17] F. Asdrubali, "A scale model to evaluate water evaporation from indoor swimming pools," *Energy & Buildings*, vol. 41, pp. 311-319, 2009.
- [18] V. Baroghel-Bouny, X. Wang, M. Thiery, M. Saillio, and F. Barberon, "Prediction of chloride binding isotherms of cementitious materials by analytical model or numerical inverse analysis," *Cement and Concrete Research*, vol. 42, pp. 1207-1224, 2012.
- [19] R. Zhang, A. Castel, and R. Francois, "Influence of steel-concrete interface defects owing to the top-bar effect on the chloride-induced corrosion of reinforcement," *Magazine of Concrete Research*, vol. 63, nr 10, pp. 773-781, 2010.
- [20] D.M. Roy, P.W. Brown, D. Shi, B.E. Sheetz, and W. May, "Concrete Microstructure Porosity and Permeability," Technical report, Strategic Highway Research Program, National Research Council, Washington, D.C., 1993.
- [21] P. Atkins and J. de Paula, "Elements of Physical Chemistry," 6th Ed., Oxford University Press, UK, 2013.
- [22] B. Martin-Perez, "Service life modelling of R.C. highway structures exposed to chlorides," PhD Thesis, Department of Civil Engineering, University of Toronto, Canada, 1999.
- [23] smhi.se.
- [24] H.Y. Moon, H. S. Kim, and D. S. Choi, "Relationship between average pore diameter and chloride diffusivity in various concretes," *Construction and Building Materials*, vol. 20, pp. 725-732, 2006.
- [25] J. Tritthart, "Pore solution of concrete: The equilibrium of bound and free chloride," *Materials and Corrosion*, vol. 60, nr 8, pp. 579-585, 2009.
- [26] M. D. A. Thomas and P. B. Bamforth, "Modelling chloride diffusion in concrete-Effect of fly ash and slag," *Cement and Concrete Research*, vol. 29, pp. 487-495, 1999.
- [27] A. Lindvall, "Chloride ingress in a Swedish road environment - five years exposure for three concrete compositions," Publication P02:4, Building Materials, Chalmers University of Technology, 2002.

swerea | **KIMAB**

Box 7047, 164 07 Kista, Sweden
Visiting Isafjordsgatan 28 A, 164 40 Kista, Sweden
+46 8 440 48 00, kimab@swerea.se, www.swreakimab.se